

IDENTIFICATION OF VISUALLY EVOKED BRAIN ACTIVITY AND CARDIAC ARTIFACT COMPONENTS THROUGH TIME-DELAYED DECORRELATION

T.H. Sander, G. Wübbeler, L. Trahms

Physikalisch-Technische Bundesanstalt
Dept. of Biosignals
Abbestr. 2-10, 10587 Berlin, Germany

A. Lueschow, G. Curio*

Universitätsklinikum Benjamin Franklin
Neurophysics Group
12200 Berlin, Germany

ABSTRACT

Applying the time-delayed decorrelation (TDD) algorithm to raw data from a visual stimulation magnetoencephalographic (MEG) experiment we investigate the viability of classification of components into artifact or stimulus related components. The TDD components associated with the cardiac artifact show a striking similarity with a Principal Component Analysis (PCA) of the averaged cardiac artifact. This could be due to a violation of the TDD assumptions by the cardiac artifact. Two TDD components have time series peaking consistently at the time expected for the primary response due to the visual stimulation, but their field maps are different from the earliest signal in the average response. An identification of TDD components with physiological sources needs further investigation.

1. INTRODUCTION

A common way of performing and analysing psycho-physiological MEG or EEG experiments consists of acquiring many epochs of supposedly similar brain activity and then calculating the average of the recorded signals with respect to the stimulus or another time point associated with the stimulus [1]. Largely unknown is the relation between the average activity and the evoked activity in the single epochs, e.g. variations of latency or source location between individual epochs seem possible. Usually such effects cannot be studied due to the noise in the raw data. Independent Component Analysis (ICA) has been suggested as a tool for the separation of evoked activity from the background noise to obtain evoked single trial signals [2, 3, 4] or to suppress artifacts [3, 5, 6, 7, 8, 9].

Applying the time-delayed decorrelation (TDD) ICA algorithm [10, 11, 12] to a continuous stream of raw MEG data under visual stimulation, we show that TDD compo-

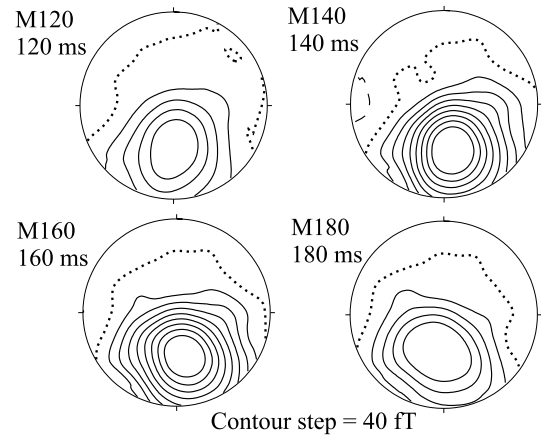


Fig. 1. Maps from a VEF averaged over 160 identical epochs are shown, which cover the earliest activity associated with the visual stimulus. A first peak is observed at 140 ms and it is considered the primary response of the inferotemporal visual cortex.

nents may have time series strongly correlated to the visual stimulus, while having clearly different field distributions compared to the field maps of the earliest response in the averaged visually evoked field (VEF). A removal of clearly identifiable components due to the cardiac artifact (CA) gives promising single epoch raw data possibly suitable for a model driven analysis using e.g. a dipole model.

2. VISUALLY EVOKED FIELDS

In twelve volunteers the visually evoked MEG response was recorded using 49 axial gradiometer channels of a planar multichannel SQUID system [13] positioned with its central sensor over T6 (defined in the 10-20 EEG electrode placement system). A sequence of grey tone images of faces arranged in a delayed-matching-to-sample-paradigm with 0, 1, or 2 intervening items were shown to the subjects. The presentation time for faces was 500 ms followed by a

* Stimulating discussions with G. Nolte, M. Burghoff, A. Ziehe, and K.-R. Müller and the usage of their software packages is gratefully acknowledged. This work is supported by the DFG grant number Ma 1782/1-4 and Cu 36/1-3.

uniformly gray image presented for 1100 ms leading to an inter-stimulus-interval of 1.6 s. A pause of 2.7 s was inserted between the individual delayed-matching-to-sample sequences.

In this paper we present data from a single subject chosen from the group of twelve for its high signal amplitudes in the VEF, which reach 400 fT at 140 ms in one channel. In Fig. 1 four maps from the VEF calculated over 160 sample-face presentations are shown.

These maps cover the first peak in the VEF associated with the primary response of the inferotemporal visual cortex and we denote the maps in the following as M120, M140, etc. The observed monopolar field pattern is fairly stable over 60 ms showing only a slight shift of the peak position. For display purposes a baseline vector defined as the average of the VEF from -200 to 0 ms was subtracted in Figs. 1 and 4, but not for any of the calculations. Due to bandpass filtering of the raw data the baseline vector was almost negligible.

3. TEMPORAL DECORRELATION

In the ICA model for stationary sources it is assumed that the recorded data are a linear superposition of n functions of the form $\vec{f}_i(t) = s_i(t)\vec{a}_i$, where $s_i(t)$ is a time dependent amplitude function statistically independent from all others and \vec{a}_i is a time independent field pattern in the m channel sensor system. For our MEG system this pattern is usually visualized as a magnetic field map of the B_z -component. Combining the $s_i(t)$ into $\vec{s}(t)$ and the \vec{a}_i into \underline{A} , the vector of the time traces $x_j(t)$ measured in the sensor channels is given by

$$\vec{x}(t) = \underline{A}\vec{s}(t). \quad (1)$$

The functions $s_i(t)$ and the associated maps \vec{a}_i are generally unknown. ICA algorithms construct a demixing matrix \underline{W}^{-1} fulfilling for the case $n \leq m$

$$\underline{W}^{-1}\vec{x}(t) = \vec{u}(t), \quad (2)$$

where the $u_i(t)$ are identical to the $s_i(t)$ disregarding an indeterminacy in scale and ordering. For the interpretation it is helpful to normalize each column \vec{w}_i of \underline{W} using the L2-norm and then to calculate the RMS amplitude of the resulting time series $u_i(t)$.

Testing for statistical independence can be done by calculating the time-lagged cross-correlation $K_{ij}(\tau)$ between $s_i(t)$ and $s_j(t + \tau)$. Under the assumption of non-zero auto correlations, statistical independence means decorrelation for all time-lags τ , i.e.

$$\langle s_i(t)s_j(t + \tau) \rangle = K_{ij}(\tau)\delta_{ij}. \quad (3)$$

This equation is the basis of the TDD algorithm [10, 11, 12], which requires the calculation of several time-delayed covariance matrices $C_{ij}(\tau_k) = \sum_i x_j'(t_i)x_j'(t_i + \tau_k)$, where $x_j'(t)$ denotes data resulting after a whitening of the original signal using PCA. These matrices are simultaneously diagonalized and the resulting rotation matrix combined with the inverted whitening matrix yields the demixing matrix \underline{W}^{-1} . For more than two matrices this diagonalization can be achieved only approximately. The TDD algorithm relies on spectral differences [11, 14], which are a reasonable assumption for the CA and the evoked activity in our experiment. Applications and variants of the TDD algorithm can be found in [6, 8, 9, 15, 16, 17, 18, 19].

4. SELECTED TDD COMPONENTS

For the TDD calculation we used 180000 raw data points from each of 49 sensor channels sampled at 500 Hz. Prior to the TDD calculation the raw data were digitally bandpass filtered between 0.4 and 40 Hz to eliminate high and low frequency noise. The number of time delayed covariance matrices was 500 with a time lag of 20 ms between successive matrices. This corresponds to a maximum time shift of 10 s, which was chosen to cover the 9 s maximum length of a delayed-matching-to-sample sequence. In [14] it was shown that the time delay operation corresponds to filtering with a sinusoidal comb filter with the comb finger distance decreasing with increasing time delay. This means that using larger time shifts can resolve smaller spectral differences. To obtain the result shown in Fig. 2 it was necessary to use a maximum time shift of 10 s. This hints at the necessity to isolate small spectral differences in our data.

In Fig. 2 selected components of the TDD calculation are shown. The component vector is visualized as a field map and a 16 s second section of the full time series of 360 s and the spectrum of this section is given. The components $CA1$ and $CA2$ are attributed to the CA due to their time series and the respective spectra. The time series show a periodic peak at intervals of 0.67 s and the spectra are dominated by the corresponding heart frequency and its harmonics ($i * 1.5$ Hz, $i = 1, 2, \dots$). The spectra of $CA1$ and $CA2$ are rather different as the spectrum of $CA2$ is dominated by the harmonics of the heart frequency, whereas the spectrum of $CA1$ shows a peak at the heart frequency and its 1st harmonic. The CA components will be discussed further in section 6.

The arrows above the time series of components $VEF1$ and $VEF2$ in Fig. 2 are positioned at 140 ms after a visual stimulus. Component $VEF2$ shows always peaks at this time, the peaks are less systematic in the time series of $VEF1$. The spectra of both components show peaks at 0.6 Hz in agreement with the inter-stimulus-interval of 1.6 s. Higher frequencies are stronger in the spectrum of $VEF2$.

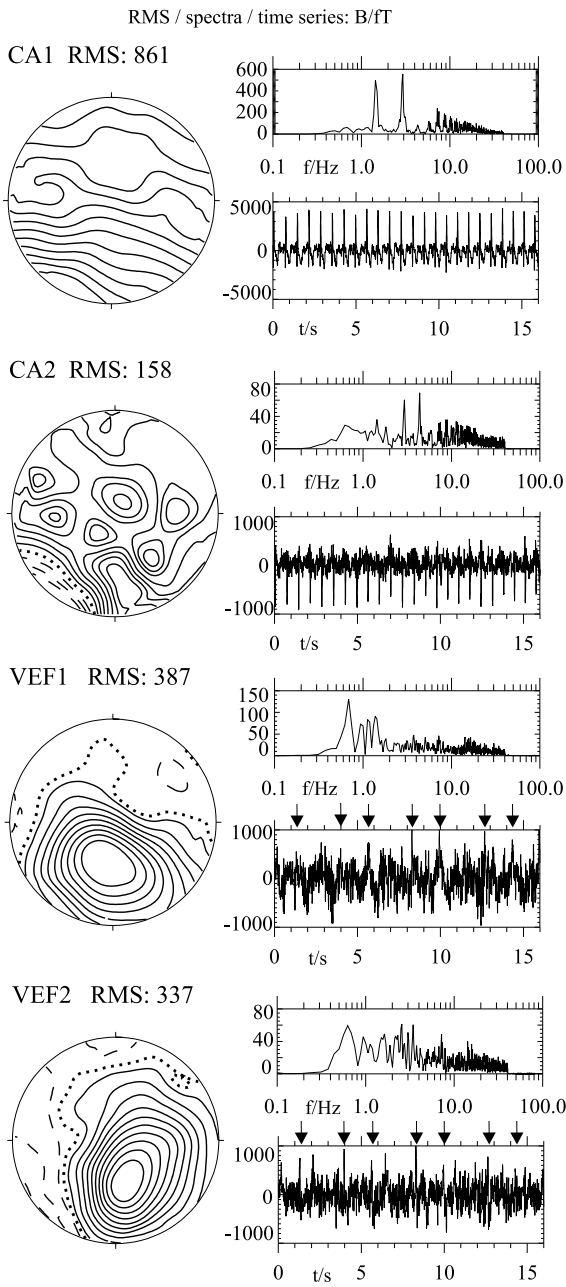


Fig. 2. Four selected components of the TDD calculation. The map of the component vector (left), a part of the full time series (top) and the spectrum of the partial time series (bottom) are shown respectively. The arrows indicate the M140 timepoints, i.e. a visual stimulus was given 140 ms before an arrow. Note that the visual stimulation was not strictly periodic. The components *CA1* and *CA2* are attributed to the heart beat (CA) and *VEF1* and *VEF2* to the visually evoked field.

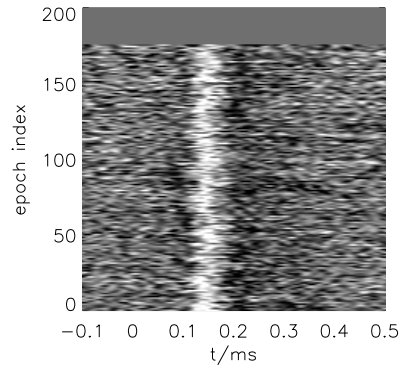


Fig. 3. Consecutive evoked epochs in the time series of *VEF2* displayed as a gray scale plot. The zero of the time scale is the start of the image presentation. A stable response to the stimulus can be seen at 150 ms.

compared to *VEF1*. This is in agreement with the sharper peaks in the time series of *VEF2* and the strong low frequency activity in the time series of *VEF1* in Fig. 2. Due to the time series and the spectra components *VEF1* and *VEF2* are attributed to the visually evoked field. This attribution is supported by Fig. 3, where slices of the time series of *VEF2* aligned at the onset of image presentation have been displayed in a gray scale plot. In most of the epochs an answer to the stimulus is observed at 150 ms. This suggests that each single visual stimulus leads to a fairly stable response of the inferotemporal visual cortex.

5. DEMIXING OF VEF USING TDD BASE

Assuming that components *VEF1* and *VEF2* are indeed related to the visual stimulus they should explain a large proportion of the averaged signal, i.e. the VEF. To test this the VEF was demixed using \mathbf{W}^{-1} , for the three strongest TDD components and the resulting time series are shown in Fig. 4. These components are the strongest in the VEF too, e.g. at 160 ms components *VEF1* and *VEF2* explain 80 % of the signal strength with respect to the L2-norm.

The time series of *VEF1* and *VEF2* are close to zero up to 50 ms after the visual stimulus, which was given at 0 s. The time series of *CA1* is clearly non-zero in this interval. At 100 ms the time series of *VEF2* shows a negative peak followed by a strong positive peak at 140 ms, which is earlier than the positive peak in the time series of *VEF1* at 160 ms. Both components are clearly related to the VEF.

The time series of component *CA1* reaches a maximum at 150 ms suggesting that it is associated with the VEF as well. This could mean that the TDD separation is incomplete, i.e. leakage between VEF and cardiac artifact components occurs, or that the VEF contains remnants of the CA despite the averaging procedure. Possibly both mech-

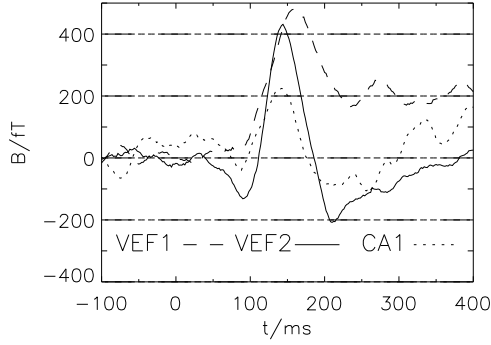


Fig. 4. Selected time series from the demixing of the VEF using the TDD base. The time series of *VEF1* and *VEF2* peak at 140 ms, the time of the primary response to the visual stimulus in the inferotemporal cortex (cf. Fig. 1). Component *CA1* has a weaker response at this time. Its time series shows weak activity even before stimulus onset in contrast to *VEF1* and *VEF2*.

anisms contribute. Nevertheless the weak non-zero signal observed before stimulus onset in the time series of *CA1* can only be explained as remnants of the CA in the VEF.

Considering that the time series of *VEF2* peaks at 140 ms after stimulus onset in Fig. 2 and that it represents partially the earliest signal in the VEF as can be seen in Fig. 4, the map of *VEF2* could be interpreted as the field pattern of the cortical source generating the primary response to visual stimuli. But the map of *VEF2* is evidently different from the M140 map in Fig. 1 as can be quantified by the angle

$$\alpha_{ij} = \arccos(\vec{VEF2}/|\vec{VEF2}| * \vec{M140}/|\vec{M140}|). \quad (4)$$

The resulting angle of 27° and the other angles in Table 1 should be seen in relation to the angle of 9° between the M140- and the M160-vectors. It becomes clear that neither *VEF2* nor *VEF1* can be associated with the M140 or the M160. Only the sum $aVEF2 + bVEF1$, where a and b are amplitude values taken from Fig. 4, is a fairly good description of the evoked signal between 140 and 180 ms.

6. PCA OF AVERAGE CARDIAC ARTIFACT

Instead of calculating the stimulus triggered average, i.e. the VEF, it is possible to calculate the cardiac R-peak triggered average, i.e. an average cardiac artifact (aCA). It gives the average field evolution measured in the MEG system due to the current distribution in the heart muscle during the heart beat. For a comparison with the TDD components we calculated the PCA of the aCA field evolution in the time range from 200 ms before to 400 ms after the R-peak. The first

Table 1. The angles between TDD component vectors from Fig. 2 and the VEF at four different times from Fig. 1. The values a and b for the linear combination are taken from Fig. 4.

	<i>VEF1</i>	<i>VEF2</i>	$aVEF1 + bVEF2$
M120	22	34	20
M140	25	27	16
M160	18	28	10
M180	12	44	13

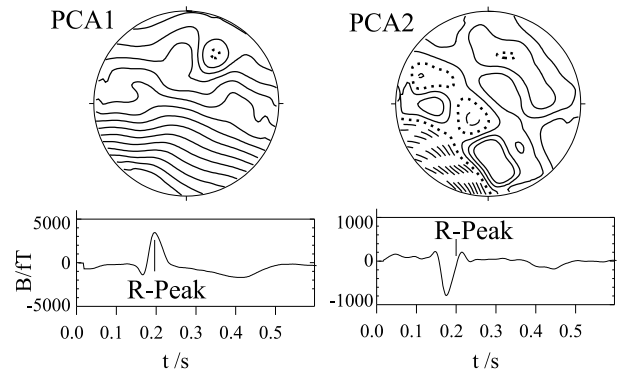


Fig. 5. The first two PCA components of the average CA. They are similar to the TDD components *CA1* and *CA2*.

two PCA component vectors are shown in Fig. 5. Component *PCA1* peaks at the R-peak position and *PCA2* peaks slightly earlier and can be associated with the Q-peak of the QRS-complex.

A similarity between the maps of *PCA1* and the TDD component *CA1* is immediately obvious and the angle α_{ij} (as defined above) between *CA1* and *PCA1* is only 4.5° . Components *CA2* and *PCA2* appear to be similar as well showing an arced gradient in the lower left part of the map, although their angle is 46° . After subtraction of a suitable offset an angle of less than 25° results between *CA2* and *PCA2*. Using fewer time-delayed covariance matrices in the TDD calculation a component similar to *CA2* is found, which has an angle of 20° with *PCA2*. This means that the TDD-algorithm applied to raw data and the PCA applied to the aCA give a similar result with respect to the CA.

For the interpretation of the TDD components the similarity between the TDD- and the PCA-base is very useful as it validates a posteriori the association of *CA1* and *CA2* with the CA.

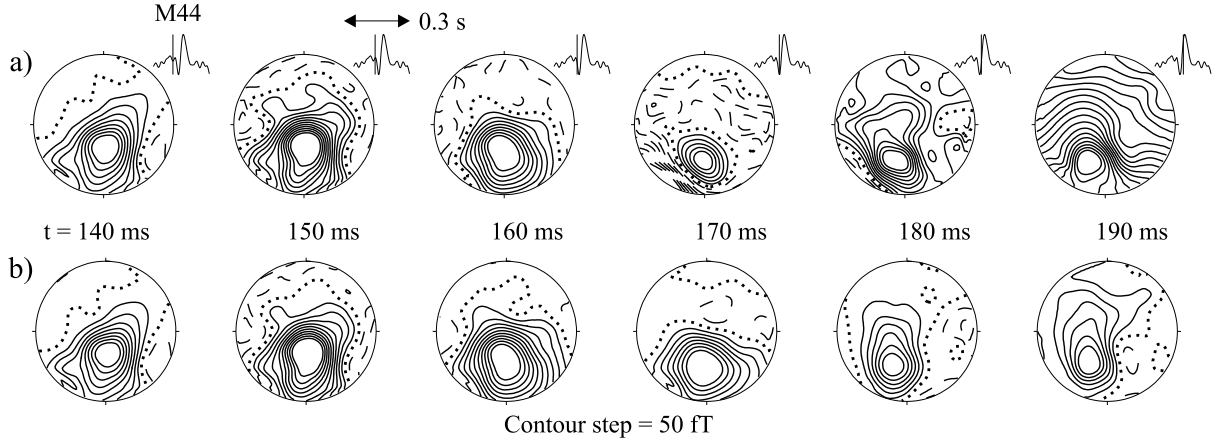


Fig. 6. Sequence of raw data before (a) and after removal (b) of the TDD components *CA1* and *CA2*. Before the removal the signal in magnetic channel M44 shows clearly the R-peak of the CA and the vertical lines indicate the position of each map relative to the R-peak. The suppression of the CA components strongly modifies the signal between 170 and 190 ms.

7. CA SUPPRESSION IN RAW MEG DATA

To obtain raw data suitable for a model-driven analysis of single-trial activity we exemplify the suppression of the CA in raw data by omission of *CA1* and *CA2* from the TDD base. The suppression is done mathematically by demixing the data using \mathbf{W}^{-1} and then recombining the data using a mixing matrix \mathbf{W}' with appropriate columns set to zero.

This suppression of *CA1* and *CA2* is shown in Fig. 6 for a short sequence of raw data starting 140 ms after a visual stimulus. This particular sequence was chosen for its proximity to an R-peak of the cardiac cycle. At the top of the figure the single sensor channel M44 is shown, which contains a strong CA contribution and which was used to detect the R-peak time instant for the calculation of the aCA. The vertical lines indicate the timepoints of each map below. After removal of *CA1* and *CA2* the R-peak is not visible anymore in M44 (not shown). In Fig. 6a) a monopolar map similar to Fig. 1 can be seen up to 160 ms. Between 170 and 190 ms the maps are clearly influenced by the R-peak of the CA. In the lower left part of the map at 170 ms in Fig. 6a) the arced field pattern of *CA2* can be seen and the gradient at 190 ms is reminiscent of *CA1*. In Fig. 6b) those two components have been suppressed and between 170 and 190 ms monopolar maps have been recovered. Comparing Fig. 6a),b) with Fig. 1 shows qualitatively that the suppression of *CA1* and *CA2* yields raw data much more similar to the average signal. The CA is important for most other evoked epochs as well due to the longer duration of P- and T-wave compared to the R-peak.

Alternatively to the omission of CA components from the TDD base a regression method based on the aCA [20] can be used to improve signal quality. The omission of TDD

components has the advantage that it can be incorporated into a subsequent model driven analysis. It is only necessary to apply the linear demixing-mixing process to the chosen model before the model parameters are estimated, e.g. transform theoretical dipole fields using the operator $\mathbf{W}'\mathbf{W}^{-1}$. Note that before applying a specific source model to raw data an appropriate baseline model is needed.

8. CONCLUSION

Applying the TDD algorithm to raw MEG data from a visual stimulation experiment we have identified two components systematically peaking at 140 ms after a visual stimulus is given. A demixing of the VEF using the TDD base calculated from unaveraged data shows that these components are an essential part of the averaged primary response to visual stimuli, but the field maps of these TDD components are different from the maps of the averaged primary response. This means that either the VEF field patterns or the TDD components or both are a simplification of the physiological activity generating the measured field. Two other TDD components are attributed to the CA. A PCA decomposition of the aCA shows that the strongest PCA component is almost identical to the strongest TDD-CA component. This similarity cannot be explained at the moment. It might be conjectured that it is a consequence of the time dependent and spatially extended current distribution in the heart producing signals in the MEG, which violate the stationarity assumption of TDD. A theoretical analysis of ICA algorithms with respect to non-stationary signals seems promising as experimental MEG data contain possibly non-stationary sources such as the CA and the spontaneous α -waves of the brain.

9. REFERENCES

- [1] T.W. Picton, O. Lins, and M. Scherg, The recording and analysis of event-related potentials, in *Handbook of Neuropsychology: Vol. 10, section 14. Event-related brain potentials and cognition* (pp. 3–73), F. Boller, J. Grafman, and R. Johnson Eds., Amsterdam:Elsevier, 1995.
- [2] T.-P. Jung, S. Makeig, M. Westerfield, J. Townsend, E. Courchesne, and T.J. Sejnowski, Analyzing and visualizing single-trial event-related potentials, in *Advances in Neural Information Processing Systems 11*, MIT press, pp. 118–124, 1999.
- [3] T.-P. Jung, S. Makeig, C. Humphries, T.-W. Lee, M.J. McKeown, V. Iragui, and T.J. Sejnowski, Removing electroencephalographic artifacts by blind source separation, *Psychophysiology*, vol. 37, pp. 163–178, 2000.
- [4] A.C. Tang, B.A. Pearlmuter, and M. Zibulevsky, Blind source separation of multichannel neuromagnetic responses, *Neurocomputing*, vol. 32-33, pp. 1115–1120, 2000.
- [5] O. Jahn, A. Cichocki, A. Ioannides, and S. Amari, Identification and elimination of artifacts from MEG signals using efficient independent component analysis, in *Recent Advances in Biomagnetism*, T. Yoshimoto et al. Eds., Tohoku University Press, pp. 224–227, 1999.
- [6] H. Ishibashi, M. Kawakatsu, M. Adachi, and M. Kotani, A basic investigation of noise reduction for MEG data using independent component analysis based on correlation function, in *Proc. of 12th Int. Conf. on Biomagnetism*, J. Nenonen, R.J. Ilmoniemi, and T. Katila Eds., Helsinki Univ. of Technology, pp. 861–864, 2001.
- [7] R. Vigário, J. Särelä, V. Jousmäki, M. Härmäläinen, and E. Oja, Independent component approach to the analysis of EEG and MEG recordings, *IEEE Trans. on Biomed. Eng.*, vol. 47, pp. 589–593, 2000.
- [8] T.H. Sander, A. Lueschow, G. Curio, and L. Trahms, Removal of α -wave artifacts in MEG data by Independent Component Analysis, in *Proc. of 12th Int. Conf. on Biomagnetism*, J. Nenonen, R.J. Ilmoniemi, and T. Katila Eds., Helsinki Univ. of Technology, pp. 857–860, 2001.
- [9] A.K. Barros and N. Ohnishi, Removal of quasi-periodic sources from physiological measurements, in *Proc. of ICA'99*, pp. 87–92, Aussois, 1999.
- [10] L. Molgedey and H.G. Schuster, Separation of a mixture of independent signals using time delayed correlations, *Phys. Rev. Lett.*, vol. 72, pp. 3634–3637, 1994.
- [11] A. Belouchrani, K. Abed-Meraim, J.-F. Cardoso, and E. Moulines, A blind source separation technique based on second-order statistics, *IEEE Trans. on Sig. Proc.*, vol. 45, pp. 434–444, 1997.
- [12] A. Ziehe and K.-R. Müller, TDSEP – an efficient algorithm for blind separation using time structure, in *Proceedings of the 8th ICANN*, L. Niklasson, M. Bodén, and T. Ziemke Eds., pp. 675–680, Springer Verlag, 1998.
- [13] D. Drung, The PTB 83-SQUID-system for biomagnetic applications in a clinic, *IEEE Trans. Appl. Supercond.*, vol. 5, pp. 2112–2117, 1995.
- [14] A. Ziehe, G. Nolte, G. Curio, and K.-R. Müller, OFI:Optimal filtering algorithms for source separation, in *Proc. of the 2nd Intern. Workshop on Independent Component Analysis and Blind Signal Separation*, P. Pajunen and J. Karhunen Eds., Helsinki, pp. 127–132, 2000.
- [15] A. Ossadtchi, S. Baillet, J.C. Mosher, and R.M. Leahy, Using mutual information to select event-related components in ICA, in *Proc. of 12th Int. Conf. on Biomagnetism*, J. Nenonen, R.J. Ilmoniemi, and T. Katila Eds., Helsinki Univ. of Technology, pp. 869–864, 2001.
- [16] K.-R. Müller, P. Philips, and A. Ziehe, *JADE_{TD}*: Combining higher-order statistics and temporal information for blind source separation (with noise), in *Proc. of ICA'99*, pp. 87–92, Aussois, 1999.
- [17] A. Ziehe, K.-R. Müller, G. Nolte, B.-M. Mackert, and G. Curio, Artifact reduction in magnetoneurography based on time-delayed second order correlations, *IEEE Trans. on Biomed. Eng.*, vol. 47, pp. 75–87, 2000.
- [18] G. Wübbeler, A. Ziehe, B.-M. Mackert, K.-R. Müller, L. Trahms, and G. Curio, Independent Component Analysis of non-invasively recorded cortical magnetic DC-fields in humans, *IEEE Trans. on Biomed. Eng.*, vol. 47, pp. 594–599, 2000.
- [19] A.C. Tang, D. Phung, B.A. Pearlmuter, and R. Christner, Localization of independent components from magnetoencephalography, in *Proc. of the 2nd Intern. Workshop on Independent Component Analysis and Blind Signal Separation*, P. Pajunen and J. Karhunen Eds., Helsinki, pp. 127–132, 2000.
- [20] K. Abraham-Fuchs, P. Strobach, W. Härrer, and S. Schneider, Improvement of neuromagnetic localization by MCG artifact correction in MEG recordings, in *Biomagnetism: Clinical aspects*, M. Hoke et al. Eds., Elsevier Science , pp. 787–791, 1992.